



Contents lists available at ScienceDirect

Tectonophysics

journal homepage: www.elsevier.com/locate/tecto

Partial melt in the upper-middle crust of the northwest Himalaya revealed by Rayleigh wave dispersion

Warren B. Caldwell^{a,*}, Simon L. Klemperer^a, Shyam S. Rai^b, Jesse F. Lawrence^a

^a Dept. of Geophysics, Stanford University, Stanford, CA 94305, USA

^b National Geophysical Research Institute, Hyderabad 500 007, India

ARTICLE INFO

Article history:

Received 29 June 2008

Received in revised form 6 December 2008

Accepted 6 January 2009

Available online xxx

Keywords:

Himalaya

Tibet

Channel flow

Surface waves

Rayleigh waves

Dispersion

ABSTRACT

Seismic shear-wave velocities are sensitive to the partial melts that should be present in the Himalayan orogen if low-viscosity channel flow is active at the present day. We analyzed regional earthquakes in the western Himalaya and Tibet recorded on 16 broadband seismometers deployed across the NW Indian Himalaya, from the Indian platform to the Karakoram Range. We used a multiple filter technique to calculate the group velocity dispersion of fundamental-mode Rayleigh waves, and then inverted the dispersion records to obtain separate one-dimensional shear-wave velocity models for five geologic provinces: the Tibetan plateau, Ladakh arc complex, Indus Tsangpo suture zone, Tethyan Himalaya, and Himalayan thrust belt. Our velocity models show a low-velocity layer (LVL) with 7–17% velocity reduction centered at ~30 km depth and apparently continuous from the Tethyan Himalaya to the Tibetan plateau. This LVL shows good spatial correspondence with observations of low resistivity from magnetotelluric studies along the same profile. Of the possible explanations for low velocity and low resistivity in the mid-crust, only the presence of melts or aqueous fluids (or both) satisfactorily explains both sets of observations. Elevated heat flow observed in the NW Himalaya implies that if aqueous fluids are present in the mid-crust, then the mid-crust is well above its solidus. Comparison of our results with laboratory measurements and theoretical models suggests 3–7% melt is present in a channel in the upper-middle crust of the NW Himalaya at the present day, and the physical conditions to enable active channel flow may be present.

© 2009 Elsevier B.V. All rights reserved.

1. Introduction

1.1. Geologic setting

The Tibetan plateau consists of a series of accreted terranes separated by sutures (e.g. Yin and Harrison, 2000) (Fig. 1a). In western Tibet, the southernmost terrane is the Ladakh arc complex, a magmatic arc formed at 70–50 Ma above the subduction zone consuming the Neo-Tethys Ocean (Weinberg and Dunlap, 2000). The Ladakh arc complex is separated from crust originating on the Indian plate by the Indus Tsangpo suture zone (ITSZ), a complex composed of oceanic crust and mantle that was emplaced on the passive continental margin of India. South of the ITSZ lies the Tethyan Himalaya, a fold-and-thrust belt of metasedimentary rocks originally deposited on the Tethyan continental margin of India. South of the Tethyan Himalaya are high-grade crystalline rocks of the Greater Himalayan Sequence (GHS). The GHS is separated from the Tethyan Himalaya by the South Tibetan Detachment (STD), a shear zone most recently exhibiting normal movement, and from the Lesser Himalayan Sequence (LHS) to the south by the Main Central Thrust (MCT), a shear zone most recently

exhibiting thrust movement. South of the LHS are the Main Boundary Thrust, Subhimalaya, Main Frontal Thrust, and the Indian platform (e.g. Yin and Harrison, 2000; Jain et al., 2003).

1.2. Tectonic models for the Himalaya and Tibet

Two end-member models exist to explain the large-scale shortening and deformation of the Himalaya: a traditional thrust belt model (e.g. Srivastava and Mitra, 1994; DeCelles et al., 2001), in which deformation is accommodated by brittle faulting and folding in the upper crust and localized ductile shear zones in the lower crust, and a channel-flow model (Grujic et al., 1996; Nelson et al., 1996; Beaumont et al., 2001), in which underthrust material from the subducting Indian plate undergoes partial melting and returns to the surface via mid-crustal flow towards the thinner, lower-elevation crust of the foreland. In the channel flow model, focused erosion along the southern slopes of the Himalaya from the Indian monsoon leads to rapid exhumation, promoting advection in the channel and a resulting southward flow of material (Beaumont et al., 2001). This material is exhumed as the high-grade crystalline rock of the GHS. In the field, the GHS is bordered by two shear zones with opposite sense of movement: in the north by the north-dipping, top-to-the-north STD, and in the south by the north-dipping, top-to-the-south MCT. Because the

* Corresponding author. Tel.: (650) 724–0461.

E-mail address: warrenc@stanford.edu (W.B. Caldwell).

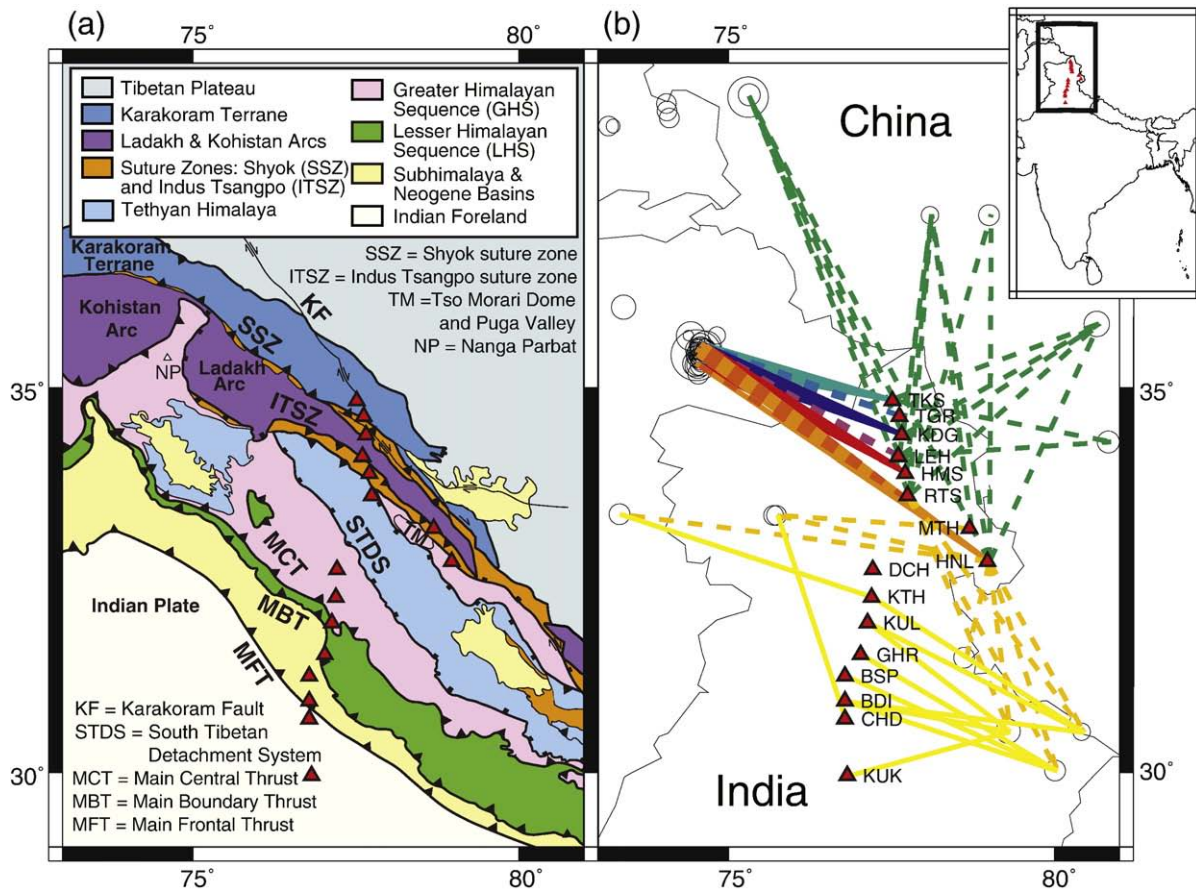


Fig. 1. (a) Station locations and regional geology, based on Goscombe et al. (2006). (b) Source–receiver ray paths and regional seismicity during station deployment. Color scheme and dashed/solid lines indicate the different regions used to group the models. The groups sample, from north to south, the Tibetan plateau (green; arrivals from the north and east at eight northern stations grouped together), Ladakh arc complex (blue and purple shades, four groups separately measured at TKS, TGR, KDG and LEH), Indus Tsangpo suture zone (ITSZ) (orange and red shades, three groups separately measured at HMS, RTS, and combining arrivals from the northwest to MTH and HNL), Tethyan Himalaya (dashed orange, combining arrivals from the south and west to MTH and HNL) and Himalayan thrust belt (GHS, LHS and Subhimalaya) (yellow; results at seven southern stations grouped together).

STD and MCT were coeval over extended geologic time (e.g. Godin et al., 2006), and because the GHS contains high-grade and pervasively sheared rocks, it has been interpreted as the surface manifestation of a viscous channel flowing southward through the mid-crust (Grujic et al., 1996). This ductile channel is also thought to contain and localize partial melts that are molten during flow and that crystallize as the High Himalayan leucogranites (e.g. Klemperer, 2006).

1.3. Previous geophysical work

Numerous geophysical studies of the Tibetan plateau (mostly focused from 85 to 95°E) support the existence of a hot and silica-rich mid- or lower crust that undergoes ductile flow on geologic time scales (e.g. Klemperer, 2006). However, significant controversy remains regarding the Indian Himalaya and western Tibet, where both geological and geophysical evidence has been used to argue for the channel flow model (Unsworth et al., 2005; Hodges, 2006) and against it (Kohn, 2008; Oreshin et al., 2008).

Magnetotelluric (MT) studies in the NW Himalaya reveal a low-resistivity layer in the mid-crust, which can be explained by partial melts, aqueous fluids or graphite (Gokarn et al., 2002; Harinarayana et al., 2004, 2005; Arora et al., 2007). These results have been regionally attributed to fluids and used to argue for ductile channel flow (Unsworth et al., 2005), but Leech (2008) argues that the resistivity is not low enough to indicate sufficient melt to reduce viscosity to levels that permit modern channel flow. Alternatively, at least locally, the low resistivities above 20 km depth have been attributed to serpentinite or

graphitic zones (Arora et al., 2007). MT data cannot distinguish between fluids (aqueous or magmatic), which would cause low-viscosity, and graphite-, serpentinite- or sulphide-rich zones, such as are commonly seen in other suture zones (e.g. Korja and Hjelt, 1999; Jones et al., 2005), and which do not imply low-viscosity (although graphite and serpentinite do cause low yield strength). In contrast, seismic observations can directly image reflections from fluid-rich zones (e.g. in eastern Tibet: Makovsky and Klemperer, 1999) or indirectly recognize small concentrations of fluids from low S-wave velocities (e.g. in eastern Tibet: Cotte et al., 1999). Although many changes in seismic velocity can reasonably be attributed to compositional changes (Christensen, 1996), large reductions in S-wave velocity almost certainly imply the presence of fluids (Hyndman and Shearer, 1989).

2. Methods

In this paper, we test for the presence of fluids and hence for a low-viscosity zone, in the mid-crust of the NW Indian Himalaya using velocity modeling based on dispersion of fundamental-mode Rayleigh waves.

We have measured the dispersion of surface waves (specifically, fundamental mode Rayleigh waves) and inverted these data to obtain one-dimensional models of shear-wave velocity structure. Surface wave dispersion is the result of long-period waves sampling deeper (and thus typically higher velocity) structures, causing velocity to vary with period: the longer-period components of a signal generally travel faster and arrive at a recording station sooner. This information can be

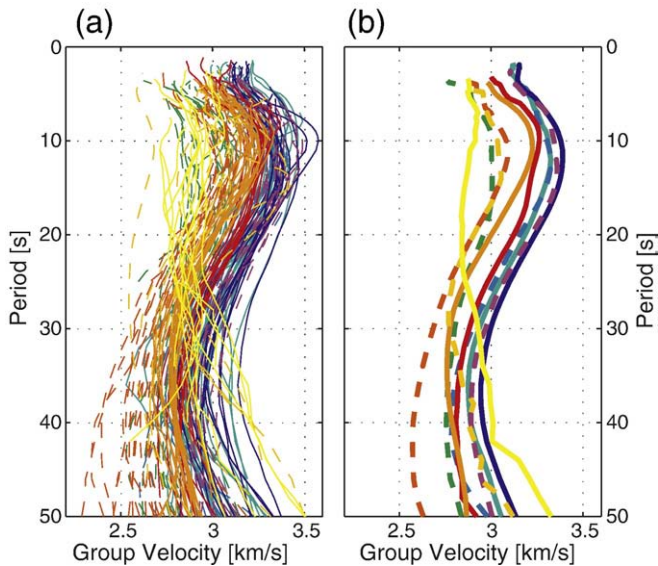


Fig. 2. (a) Dispersion curves for the 140 source–receiver pairs used in this study, after discarding any dispersion curves more than two standard deviations from the regional mean at any depth. Color scheme and dashed/solid lines follow Fig. 1b. (b) Mean dispersion curve for each region.

used to reveal velocity structure at depth (e.g. Oliver, 1962). Because shear-wave velocity is particularly sensitive to the presence of fluids, any significant fluids or partial melts present in the mid-crust should be observable as a low-velocity layer (LVL).

2.1. Data

Our data consisted of 12 months (2002–2003) of three-component broadband earthquake recordings from an array in NW India (Fig. 1; Rai et al., 2006). The array was deployed along the HIMPROBE transect, part of an Indian national project to create a geological and geophysical transect across the Himalaya (Jain et al., 2003). The Indian National Geophysical Research Institute (NGRI) operated the majority of the array, with one station (HNL) operated by Cambridge University. Sixteen stations (a mix of Guralp 3T and Guralp 3ESP seismometers) comprised the array, which ran approximately north–south for 500 km with an average station spacing of 35 km. The array traversed the Himalaya roughly orthogonal to the orogen, extending from the foreland basin to the Karakoram Range. Four stations lay north of the ITSZ, four were within or near the ITSZ, and eight were south of the ITSZ. The four ITSZ stations were laterally separated along the suture zone, and bracketed the Tso Moriri north Himalayan gneiss dome and Puga valley geothermal field (Harinarayana et al., 2004, 2005).

We used records of 36 earthquakes, choosing only events near to the array (~300–900 km source–receiver distance) in order to minimize the effects of path averaging. A dispersion curve represents average velocities over the length of the source–receiver path, so short paths provide greater spatial resolution than long paths. However, these paths were still long enough to be representative of the regional crust, so the criticism (e.g. Harrison, 2006) that geophysical studies in southern Tibet providing evidence in support of channel flow were located in anomalous rift valleys does not apply here. The seismicity of the region was not evenly spatially distributed: during the deployment, a large concentration of events occurred northwest of the array near the Nanga Parbat syntaxis (Fig. 1b).

2.2. Dispersion curve calculation

We picked several hundred group velocity dispersion curves from these events using a multiple filter technique (MFT) (Dziewonski et al.,

1969). MFT consists of bandpass filtering each seismogram around a set of frequencies, calculating the envelope function for each of the filtered signals, and manually picking the time of maximum energy arrival for each frequency. Time and velocity are equivalent (because the source–receiver distance is fixed), so this process reveals variations in amplitude as a function of period and velocity, and hence, dispersion. We use the MFT technique as implemented by Herrmann and Ammon (2002). Before applying the MFT, we removed the mean, trend, and instrument response of the seismograms and applied a taper (Dziewonski et al., 1969). The majority of the dispersion curves could be picked between 2 and 50 s, roughly corresponding to sensitivity between 3 and 75 km depth. After picking, we discarded unreliable or noisy records based on visual inspection of the bandpass-filtered seismograms.

2.3. Regional sorting

In order to investigate north–south variation, we isolated 192 dispersion curves with ray paths approximately parallel to the orogen, and divided them into ten sets corresponding to separate regions (Fig. 1b). Within each regional set, we discarded any dispersion curves that deviated from the mean of the set by more than two standard deviations, thus removing potentially spurious data (the necessarily subjective nature of manually picking dispersion curves is likely to result in some inaccuracies). This process removed 52 outlying curves, leaving 140 consistent dispersion curves. The number of accepted curves per set varied between 11 and 20. The 140 dispersion curves are shown in Fig. 2a (each colored according to its region in Fig. 1b). Within each set we took the mean group velocity at each period for which there were three or more data points, yielding an average dispersion curve for the set (Fig. 2b), and hence for the corresponding region (Fig. 1b).

2.4. Inversion

We inverted the average dispersion curve of each region to obtain one-dimensional shear-wave velocity profiles, also using an implementation of Herrmann and Ammon (2002). The earth model was parameterized with layer thicknesses of 1 km in the upper 6 km, 2 km from 6 to 50 km depth, and 5 km from 50 to 100 km depth. The inversion ran to a depth of 100 km, and although we lack resolution at that depth, doing so avoided forcing structure to artificially shallow depths. The majority of the dispersion curves could be picked to 50 s, so we interpreted only the upper 75 km of the inversion results. This corresponds to the approximate crustal thickness at the northern eight stations (Rai et al., 2006); for this reason we did not force a velocity jump at a Moho discontinuity in any of our inversions.

As with most geophysical data, the inversion is non-unique, so in order to fully characterize the range of possible solutions, we performed numerous inversions for a range of starting models and damping factors (the two parameters that most strongly influenced the inversion results) and analyzed the resulting suite of best-fitting models.

For each of our ten subsets of data, we ran 110 inversions in a grid search, representing all combinations of 5 damping factors and 22 starting models. To select the 5 damping factors, we plotted model fit vs. damping factor (an L-curve) in a standard tradeoff analysis to determine the smallest damping factor that did not significantly reduce the quality of fit—the “corner” of the L-curve (e.g. Aster et al., 2005). We then selected 5 damping factors that included and bracketed this corner point. Our 22 starting models bound and evenly spanned the range of velocities seen in the inverted models. The starting models had one of three velocity gradients (0.01 km/s/km, 0.005 km/s/km, or constant velocity), and ranged from 2.8–4 km/s at the surface and 3.2–4.6 km/s at 100 km depth.

This grid search process resulted in 110 shear-wave velocity profiles for each region. Within each region we averaged the profiles using a weighted mean with weighting $w=1/\sigma^2$, where σ was the

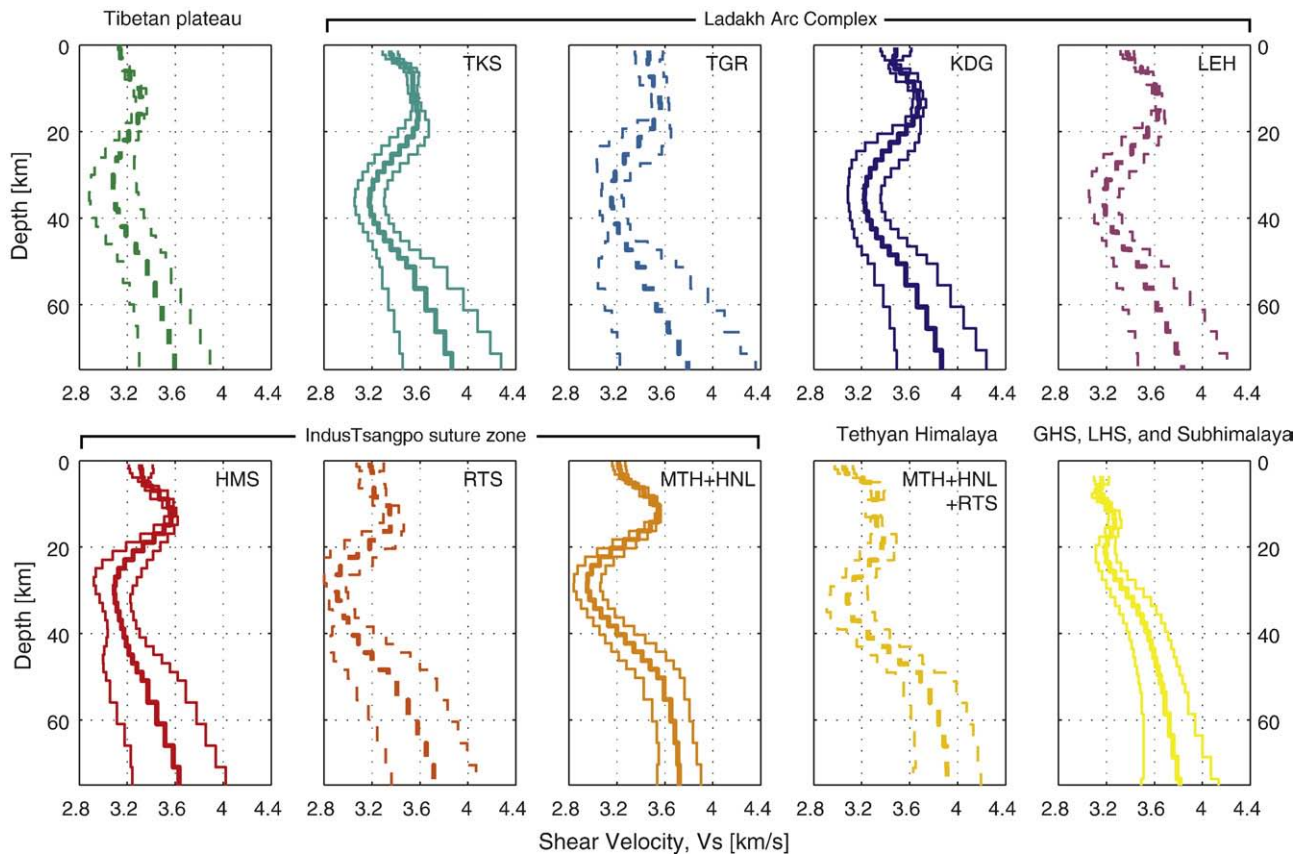


Fig. 3. Shear-wave velocity models obtained for each region. Color scheme and dashed/solid lines follow Fig. 1b. For each region, the bold line is the mean of the suite of models generated by a range of inversion parameters (see section 2.4). The mean is weighted by each model's fit to the observed dispersion data. Thinner lines show $\pm 2\sigma$ weighted standard deviation.

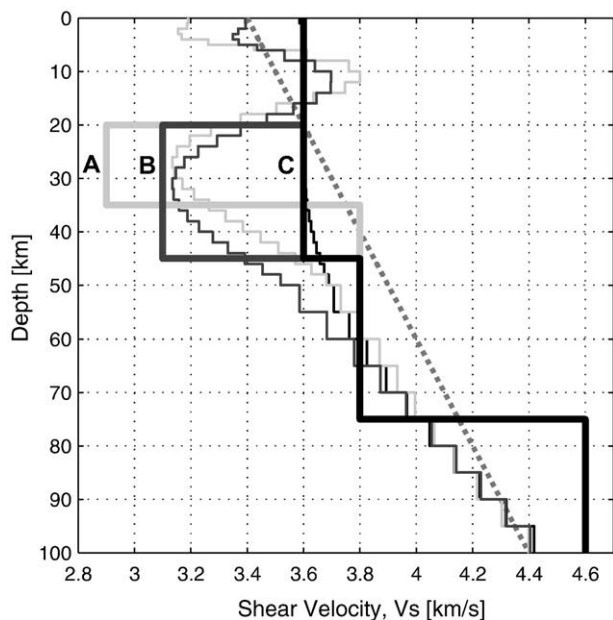


Fig. 4. Comparison of synthetic earth models (bold lines) with the corresponding inverted models (thin lines; obtained by forward calculating dispersion for each synthetic and inverting to obtain a velocity model). Gray line is the starting model for each inversion. For any observed velocity profile, a non-unique set of earth models (such as A and B in the figure) are all valid interpretations, and depend on the assumed actual thickness of the low-velocity layer (LVL). In these synthetics, the earth velocity in the LVL is always lower than the minimum velocity in the inversion.

standard error between the observed dispersion and the forward-calculated dispersion for each model. Fig. 3 shows the average model for each region with ± 2 weighted standard deviations. These bounds constrain the range of likely models and constitute our solutions for the shear-wave velocity in the NW Himalaya.

Statistically analyzing a range of possible models removes the bias, and the largest source of uncertainty, that would otherwise result from inverting with a single starting model and single damping factor. Other sources of uncertainty include the possibility that poor quality or unrepresentative seismograms may have been included, though we lessen this potential error by discarding outlying dispersion curves. The time, and hence the velocity, identified at each period by the MFT program has an inherent uncertainty, and picking errors may occur. These factors were not incorporated into the reported uncertainty bounds, though one test we conducted indicated that uncertainty in calculating the mean dispersion curve contributes an uncertainty of ± 0.05 km/s to the inverted models.

2.5. Synthetic tests

We also analyzed the resolution of our inversions by calculating synthetic dispersion curves from known earth models, performing a single (non-grid search) inversion, and comparing the inverted models to the known models (Fig. 4). These tests illustrate the non-uniqueness of the inversion: trading off thickness and velocity of an LVL (A and B in Fig. 4) can generate the same inverted model within our uncertainties. Additionally, the smoothing employed means that our inversions cannot accurately reproduce abrupt velocity changes—a smoothly varying velocity profile does not necessarily indicate smoothly varying velocities in the earth. Thus, we cannot constrain the geometry of an LVL from our results alone, and lacking constraints

on geometry from other data, we cannot infer a sharply-bounded layer, nor can we distinguish between a low-velocity thick layer and a very-low-velocity thin layer (e.g. models A and B in Fig. 4). However, we can distinguish between the presence and absence of an LVL: when the synthetic model does not contain an LVL (C in Fig. 4), no LVL is observed in the inverted model.

3. Results

3.1. Shear-wave velocity models

The velocity models (Figs. 3 and 5) all show a pronounced intra-crustal LVL. The velocities decrease starting at depths of 10–15 km (although our synthetic tests shown in Fig. 4 suggest that for a sharply-bounded channel, the actual top of the LVL could be ~10 km below this point) and reach a minimum at 28–35 km depth. The minimum velocities in each model range from 2.9 to 3.3 km/s, with the lowest velocities occurring in the vicinity of the ITSZ. The exception is the southernmost region, the Himalayan thrust belt, which has a less-pronounced LVL that reaches a minimum at 20 km depth and then increases with depth. We lack sufficient earthquake paths in this region (see Fig. 1b) to identify the location of the southern limit of the LVL, but it must extend well south of the ITSZ.

In order to interpret the nature of the LVL, we estimated the degree of velocity reduction with respect to estimates of unmodified crust. Using a constant velocity beneath the upper-crustal velocity peak as an estimate of the velocity of unperturbed crust (V_s^0 ; vertical dashed line in Fig. 5, and equivalents calculated separately for each velocity profile, with the exception of the Himalayan thrust belt), the minimum velocities in each region show a V_s reduction (ΔV_s) of between 7% (Tibetan plateau) and 17% (Tethyan Himalaya).

As described in section 2.5, the smoothing incorporated in this inversion limits our ability to infer the geometry of the LVL from these results. Our reported 2σ bounds (Fig. 3) constraining the likely range

of actual velocities allows for a variety of possible geometries, but in all cases (except the Himalayan thrust belt), an LVL is required to fit the data. If the LVL is equated with the ductile channel of the channel-flow model (e.g. Beaumont et al., 2004) we can infer likely constraints on the geometry, since the putative crustal channel is structurally bounded, above by the South Tibetan Detachment and below by the Main Himalayan/Main Central Thrust, and has a thickness that may be on the order of 25 km beneath the ITSZ (see e.g. Makovsky et al., 1999, their Plate 2).

3.2. Comparison with previous results

3.2.1. NW Himalaya

Rai et al. (2006), using the same stations as this study, jointly inverted 15–60 s Rayleigh wave group velocities with receiver functions from teleseismic arrivals, with a main focus on Moho depth and less emphasis on resolution in the mid-crust. The Rayleigh-wave inversions used by Rai et al. (2006) to stabilize their receiver-function inversions were only calculated for one of the stations used in this study (HNL), plus other more distant stations, and the Rayleigh inversions used no separation of source–receiver azimuths to isolate different geological regimes. Even with this approach, LVLs are present in their models at ~40–45 km depth for some of the ITSZ stations, and particularly in Ladakh.

Rai et al. (2009), also using the same stations as this study, modeled seismic attenuation using the Lg wave and found high attenuation in Ladakh ($Q_0 \sim 70$) and low attenuation in the Tethyan Himalaya and Himalayan thrust belt ($Q_0 \sim 700$). They interpret the high attenuation in Ladakh to aqueous fluid/partially molten crust associated with the ~21 Ma Baltoro granite.

Oreshin et al. (2008), also using the same stations as this study, modeled V_p and V_s for the crust and mantle using teleseismic body waves. Like us, they found no significant crustal LVL for the stations south of the Tethyan Himalaya, and like us they found a mid-crustal LVL associated with four stations in the ITSZ (HNL and MTH and, less clearly, HMS and RTS). North of the ITSZ, their results differ from ours: they found a lower-crustal (rather than mid-crustal) LVL at KDG in Ladakh; they were unable to analyze LEH due to “anomalous” data (for us, LEH provided reliable data, but MTH provided minimal data and DCH provided none); and they presented results showing no crustal LVL for TKS and TGR in Ladakh. Only these two northernmost stations showed no crustal LVL. Thus, although Oreshin et al. write: “The absence of a continuous crustal low-velocity layer makes channel flow unlikely in Ladakh,” we suggest that their conclusion is inappropriate given that the majority of stations they analyzed do show an LVL, and given that their inversion technique, which searches a model space consisting of ~30 km thick layers in the crust, may have been too coarse to identify an LVL beneath all stations.

3.2.2. Southern Tibet

Dispersion analyses in Southern Tibet using the INDEPTH seismic transect at c. 90°E identify an LVL in the mid-crust north of the ITSZ, and upper-middle crust south of the ITSZ (Cotte et al., 1999; Rapine et al., 2003). Cotte et al. (1999) divided their data into south-of-the-ITSZ, where they found shear velocities as low as 3.2 km/s at 10–30 km depth, and north-of-the-ITSZ, where they found an LVL of as low as 3.1 km/s at 35–55 km. These low velocities fall within the range that we observed, but our LVL depth was only slightly deeper, not significantly deeper, north of the ITSZ than south of it, and the variation is within our uncertainty. Rapine et al. (2003) used a more spatially extensive data set north of the ITSZ (their Lhasa terrane model), and found a shallower (20–40 km), less-pronounced LVL (as low as 3.25 km/s). Our observed LVLs occur at this same depth, and this velocity is within our uncertainty for regions north of the ITSZ (Fig. 3). Thus our results for the NW Himalaya show no significant distinction from published velocity data from the eastern Himalaya.

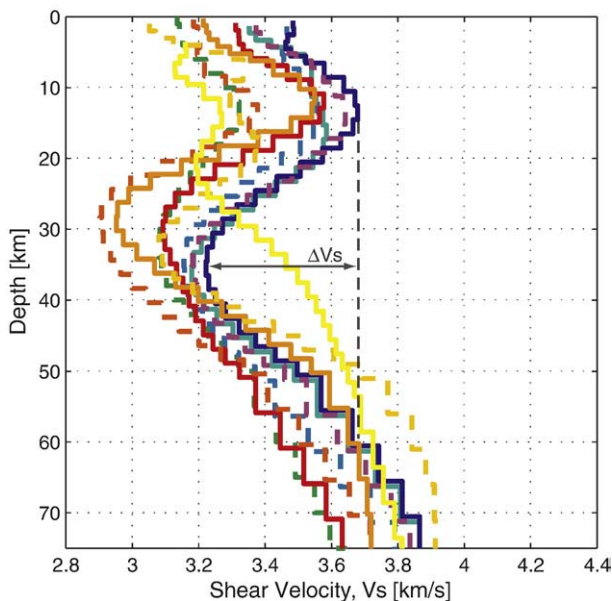


Fig. 5. Mean shear-wave velocity models obtained for each region. Color scheme and dashed/solid lines follow Fig. 1b. Depth axis is referenced to 4.5 km above sea level. All source–receiver paths (except those in the Himalayan thrust belt; yellow) have a low-velocity layer (LVL) at 20–40 km. Horizontal arrow labeled ΔV_s shows the proportional velocity reduction within the LVL with respect to the peak upper-crustal velocity (dotted vertical line). ΔV_s and peak upper-crustal velocity are shown for one velocity profile, but were calculated separately for each velocity profile.

4. Discussion

4.1. What causes the LVL?

The low velocities observed (2.9–3.3 km/s at 30 km depth) cannot be explained by the presence of solid (melt-free), dry crustal rocks of plausible composition. In the compilation of experimentally-measured shear-wave velocities of Christensen (1996), at room temperature and 1000 MPa (the approximate lithostatic pressure at 30 km depth), the metamorphic rocks with the lowest shear-wave velocities were metagraywacke, 3.51 km/s; phyllite, 3.61 km/s; granite gneiss, 3.63 km/s; biotite (tonalite) gneiss, 3.64 km/s; mica-quartz schist, 3.65 km/s; and paragranelite, 3.66 km/s. The lowest-velocity plutonic rock (granite–granodiorite) had a room-temperature velocity of 3.73 km/s at this pressure.

In order to extrapolate these velocities to mid-crustal temperatures, we used a V_s decrease of 0.2 m/s/°C, the average value determined from a range of gneisses by Kern et al. (2001). Temperature in the mid-crust of the Himalaya can be inferred from the summary of Jamieson et al. (2004) of the results of measurements (based on metamorphic grade) of peak temperature for GHS rocks in central Nepal. They found that almost all values lie between 550 and 800 °C, though the majority were between 600 and 700 °C. Although metamorphic temperatures necessarily represent past conditions, we can also compare temperature estimates from actualistic two-dimensional finite-element models of India underthrusting Tibet. Steady-state kinematic models (e.g. Cattin et al., 2001) or coupled thermal–mechanical models (Beaumont et al., 2004) predict modern peak crustal temperatures in the core of the orogenic wedge just above the MHT of 650° to 900° at c. 40 km depth at the Indus Tsangpo suture, decreasing southwards. At a gradient of 0.2 m/s/°C, these temperatures are not high enough to bring the room temperature laboratory-measured values cited above into the range of velocities that we observe. Thus, at the expected temperatures and pressures at 30 km depth in this region, no dry metamorphic or plutonic rocks can explain the observed low velocities.

The most plausible explanation for the LVL is therefore the presence of partial melts, aqueous fluids, or both, since these are easily capable of producing the observed velocity decrease of 7–17% (Watanabe, 1993; Takei, 2000), and have been frequently proposed as an explanation for low-velocity, low-resistivity, high-reflectivity geophysical anomalies in Tibet and the Himalaya (Nelson et al., 1996; Makovsky and Klempner, 1999; Li et al., 2003; Unsworth et al., 2005).

4.2. What type of fluids?

The question of which type(s) of fluids are responsible (partial melts, saline fluids, or a combination) is best addressed by considering crustal temperature in the region. Geothermal exploration of the Puga region in NW India (within the Tso Morari Dome, see Fig. 1) produced heat flow measurements of >500 mW/m² (Shanker et al., 1976), and even away from this extreme anomaly, wide-spread hot-spring activity extends from the Karakoram Fault south across NW India to the Main Boundary Thrust (e.g., Thussu, 2002). Wang (2001) estimated a regional heat flow (after correction for convective heat flow) for southern Tibet of c. 82 mW/m², equivalent to the ‘characteristic Basin and Range’ heat flow of Lachenbruch and Sass (1977), for which they calculated temperatures of 650–850 °C at 30 km depth. This is consistent with the peak temperatures inferred from geodynamic modeling (Beaumont et al., 2004) and reported by Jamieson et al. (2004) for GHS rocks. These temperatures are in excess of the pelitic wet solidus (Thompson and Connolly, 1995), implying that if aqueous fluids are present, then partial melts are almost certainly present as well. Partial melts in the absence of aqueous fluids are unlikely, because dry crustal rocks do not begin to melt until temperatures >900 °C (Litvinovsky et al., 2000). Hence wet melts are the likely cause of the observed LVL.

Partial melts have been proposed as an explanation for the low-resistivity magnetotelluric anomalies observed in the NW Indian Himalaya and elsewhere in Tibet (Unsworth et al., 2005; Arora et al., 2007), and our LVL shows good spatial correspondence in depth with the low-resistivity anomaly observed along a portion of the HIMPROBE transect (Fig. 6). Inversion of magnetotelluric data, like inversion of dispersion data, is smoothed, and these results unfortunately cannot be used to define the geometry of the LVL. Nevertheless, the spatial correspondence implies a common cause. Alternative explanations for low resistivity include graphitic schists, which have low resistivity and occur in some suture zones (e.g. Korja and Hjelt, 1999; Jones et al., 2005), but do not have pronounced low shear-wave velocity.

4.3. How much melt?

In order to constrain the percentage of melt present in the NW Indian Himalaya, we compared our shear-wave velocities with theoretical and experimentally-derived relationships between V_s and melt percentage (Fig. 7). In order to relate our results to these studies and

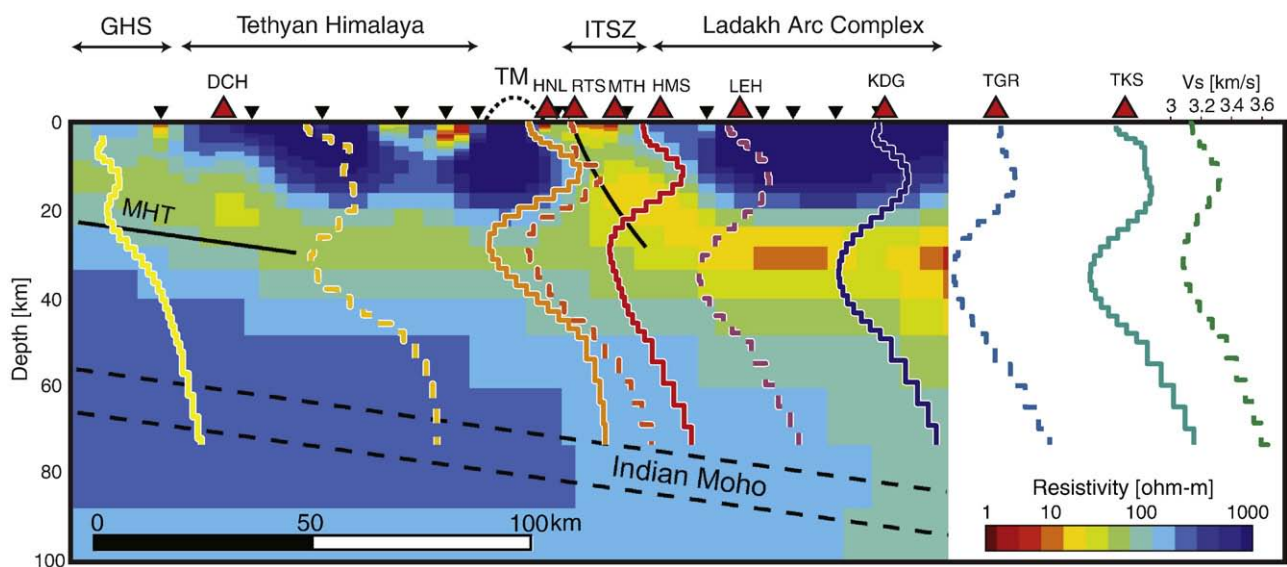


Fig. 6. Seismic stations and velocity models (from Fig. 5) projected onto the MT profile of Arora et al. (2007). Color scheme and dashed/solid lines follow Fig. 1b. The low-velocity layer (LVL) in our models shows good spatial correspondence with the low-resistivity layer inferred from the MT data. Downward-pointing triangles: MT stations of Arora et al. (2007). Upward-pointing triangles: our seismic stations. Both sets of stations were deployed along the same roads, with the exception of seismic stations MTH and HNL, 100 km southeast along strike. MHT and Indian Moho locations are the interpretations of Arora et al. (2007) and Rai et al. (2006), respectively.

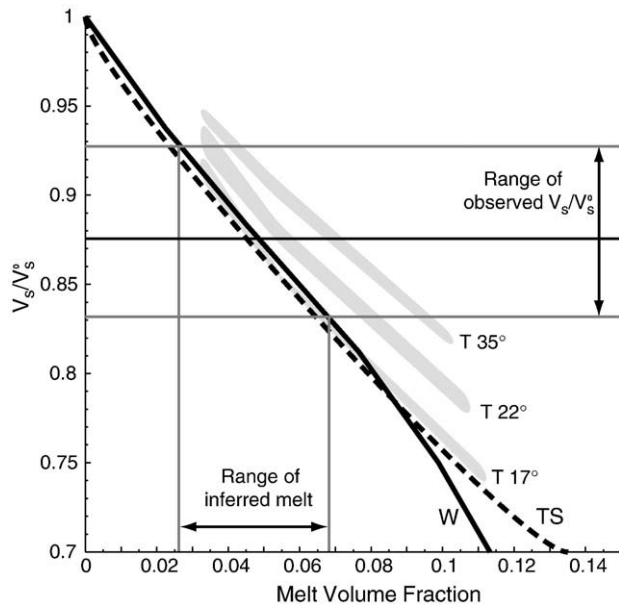


Fig. 7. Proportional velocity reduction (V_s/V_s^0) vs. melt volume fraction. Horizontal lines indicate proportional velocity reductions in the low-velocity layer (LVL) for the regions with maximum, minimum and median V_s/V_s^0 ratios (excluding the Himalayan thrust region). W: black line is analytical relationship of Watanabe (1993) for randomly oriented triangular melt tubes. T: gray relationships are the analogue experimental results of Takei (2000) for three different wetting angles, 17, 22 and 35°. TS: dashed line is analytical relationship of Taylor and Singh (2002) for the slow propagation direction in a medium containing perfectly aligned oblate spheroids of aspect ratio 10.

consider only the effects of melt volume fraction, not composition (which is unknown here), we used the ratio of V_s to V_s^0 , where V_s^0 is the shear velocity of unmodified, unmelted crust. As estimates of unmelted rock velocity V_s^0 we used, as discussed above (section 3.1), the upper-crustal peak velocity for each velocity profile (Fig. 5). We then calculated the minimum value of V_s/V_s^0 within the LVL for each region. Fig. 7 shows the median (0.88, station KDG), maximum (0.93, Tibetan plateau) and minimum (0.83, Tethyan Himalaya) of these ratios. These ratios can also be expressed as percentage velocity reduction, which yields 7–17%. This is the range of velocity reductions that we interpret for the LVL in the NW Himalaya.

We compared our V_s/V_s^0 ratios to two studies on the relationship between V_s and melt fraction (Fig. 7). Takei (2000) determined the relationship experimentally using organic analogues, and considered 3 different wetting angles in his experiments (17°, 22° and 35°). Watanabe (1993) calculated an analytical relationship for silicate melts using randomly-oriented triangular melt tubes. This relationship corresponds very well with the lowest wetting-angle experiments of Takei (2000). Comparing these relationships with our observed velocity reductions in the NW Himalaya indicates the presence of 3–7% melt (Fig. 7). If we consider our lowest observed V_s/V_s^0 ratio and higher wetting angles, the melt percentage may be as much as 10%.

We have not thus far considered possible anisotropy, which is a potential complication in analyzing the amount of melt required to produce the observed low seismic velocities. Although shearing within a sub-horizontal layer does not by itself change the average shear velocity of rock (Jones and Nur, 1984), it can create anisotropy that may make the vertical wavespeed (that dominantly sensed by Rayleigh waves) slower than the horizontal wavespeed. Published observations suggest crustal anisotropy equivalent to $\pm 4\%$ over a 30 km thick layer in central Tibet (Shapiro et al., 2004), and $\pm 10\%$ over a 6 km layer in the Himalaya of eastern Nepal (Schulte-Pelkum et al., 2005). Similar magnitude anisotropy within our observed LVL in NW India would create less than half of our observed V_s/V_s^0 anomaly of 7–17%. Although we do not know of physical measurements of seismic

wavespeed in sheared partially molten rocks, theoretical calculations of velocity reduction in media containing horizontally-aligned melt-filled cracks (Taylor and Singh, 2002) are also shown in Fig. 7 and imply that even anisotropic media require significant melt to create our observed velocity reduction.

4.4. Is there channel flow?

The numerical models of Beaumont et al. (2004) require an order of magnitude viscosity drop to induce channel flow, and the experimental results of Rosenberg and Handy (2005) indicate that an order of magnitude drop in rock strength occurs between 0 and 7% melt. Unsworth et al. (2005) identified 5–14% melt in southern Tibet and 2–4% in NW India based on MT measurements, and suggested that this creates a sufficiently large viscosity drop to allow for channel flow in southern Tibet and less-well-developed channel flow in the NW Himalaya.

Our preferred interpretation is that 3–7% partial melt is present in the NW Himalaya, more than has been suggested on the basis of MT results, but still less than is implied for southern Tibet by MT data. This amount of melt makes channel flow in western Tibet and the NW Himalaya possible, but not certain. Major uncertainties in determining absolute melt fraction from our velocity results include the unknown thickness of the LVL (that could raise the inferred melt percentage), possible anisotropy (that would most likely reduce the inferred melt percentage), and the unknown composition of the LVL and the likely variation of crustal composition with depth (that could either raise or lower the inferred melt percentage).

Although we might choose to infer greater velocity reduction (and hence higher melt percentages and lower viscosities) by supposing the velocity anomaly to be confined to a thinner channel (as in model A in Fig. 4), this does not necessarily create a stronger argument for significant channel flow occurring at the present day. Clark and Royden (2000) showed that material flux in a channel varies with h^3/μ (where h is thickness and μ is viscosity), so thin, low-viscosity channels do not necessarily allow greater mass transfer than thicker, marginally higher-viscosity channels.

5. Conclusions

Our preferred interpretation is of 3–7% partial melt *in situ* at the present day beneath and north of the South Tibetan Detachment in the mid-crust of the Himalaya and Tibetan plateau of NW India. The region of low velocities appears to deepen slightly to the north and continues north of the Karakoram fault, beyond the region yet sampled by MT data in western Tibet. The LVL also persists south of the ITSZ in a region where existing MT data shows lower conductivities than further north. Our observations of an LVL confirm earlier speculations based only on MT data about a low-viscosity layer beneath the NW Himalaya, and are consistent with a southward-shallowing, mid-crustal ductile channel that may be active at the present day (cf. Beaumont et al., 2004). Our data show that the LVL is diminished or absent further south beneath the Lesser Himalaya, hence melts must be absent (or solidified) there, but the southern limit of the LVL is currently poorly defined. Additional geometrical constraints on possible structural boundaries to the LVL, or on the composition of and anisotropy within the LVL, would greatly increase the reliability of our estimates.

Acknowledgements

Djordje Grujic, Martyn Unsworth and an anonymous reviewer provided valuable comments. Cambridge University operated one of the stations used in this study and generously allowed use of their data. Stanford University provided funding for WC. NSF grant 04-09939 further supports Stanford studies of Tibet.

References

- Arora, B.R., Unsworth, M.J., Rawat, G., 2007. Deep resistivity structure of the northwest Indian Himalaya and its tectonic implications. *Geophysical Research Letters* 34, L04307. doi:10.1029/2006GL029165.
- Aster, R.C., Borchers, B., Thurber, C.H., 2005. *Parameter Estimation and Inverse Problems*. Elsevier Academic Press.
- Beaumont, C., Jamieson, R.A., Nguyen, M.H., Lee, B., 2001. Himalayan tectonics explained by extrusion of a low-viscosity crustal channel coupled to focused surface denudation. *Nature* 414 (6865), 738–742. doi:10.1038/414738a.
- Beaumont, C., Jamieson, R.A., Nguyen, M.H., Medvedev, S., 2004. Crustal channel flows: 1. Numerical models with applications to the tectonics of the Himalayan-Tibetan orogen. *Journal of Geophysical Research* 109, B06406. doi:10.1029/2003JB002809.
- Cattin, R., Martelet, G., Henry, P., Avouac, J.P., Diament, M., Shakya, T.R., 2001. Gravity anomalies, crustal structure and thermo-mechanical support of the Himalaya of Central Nepal. *Geophysical Journal International* 147 (2), 381–392. doi:10.1046/j.0959-540x.2001.01541.x.
- Christensen, N.I., 1996. Poisson's ratio and crustal seismology. *Journal of Geophysical Research* 101 (B2), 3139–3156.
- Clark, M.K., Royden, L.H., 2000. Topographic ooze: building the eastern margin of Tibet by lower crustal flow. *Geology* 28 (8), 703–706.
- Cotte, N., Pedersen, H., Campillo, M., Mars, J., Ni, J.F., Kind, R., Sandvol, E., Zhao, W., 1999. Determination of the crustal structure in southern Tibet by dispersion and amplitude analysis of Rayleigh waves. *Geophysical Journal International* 138 (3), 809–819. doi:10.1046/j.1365-246x.1999.00927.x.
- DeCelles, P.G., Robinson, D.M., Quade, J., Ojha, T.P., Garzzone, C.N., Copeland, P., Upreti, B.N., 2001. Stratigraphy, structure, and tectonic evolution of the Himalayan fold-thrust belt in western Nepal. *Tectonics* 20 (4), 487–509.
- Dziewonski, A., Bloch, S., Landisman, M., 1969. A technique for the analysis of transient seismic signals. *Bulletin of the Seismological Society of America* 59 (1), 427–444.
- Godin, L., Grujic, D., Law, R.D., Searle, M.P., 2006. Channel flow, ductile extrusion and exhumation in continental collision zones: an introduction. *Geological Society, London, Special Publications* 268 (1), 1–23. doi:10.1144/GSL.SP.2006.268.01.01.
- Gokarn, S.G., Gupta, G., Rao, C.K., Selvaraj, C., 2002. Electrical structure across the Indus Tsangpo suture and Shyok suture zones in NW Himalaya using magnetotelluric studies. *Geophysical Research Letters* 29 (8), 1251. doi:10.1029/2001GL014325.
- Goscombe, B., Gray, D., Hand, M., 2006. Crustal architecture of the Himalayan metamorphic front in eastern Nepal. *Gondwana Research* 10 (3–4), 232–255. doi:10.1016/j.gr.2006.05.003.
- Grujic, D., Casey, M., Davidson, C., Hollister, L.S., Kündig, R., Pavlis, T., Schmid, S., 1996. Ductile extrusion of the Higher Himalayan Crystalline in Bhutan: evidence from quartz microfabrics. *Tectonophysics* 260 (1–3), 21–43. doi:10.1016/0040-1951(96)00074-1.
- Harinarayana, T., Abdul Azeez, K., Naganjaneyulu, K., Manoj, C., Veeraswamy, K., Murthy, D., Prabhakar Eknath Rao, S., 2004. Magnetotelluric studies in Puga valley geothermal field, NW Himalaya, Jammu and Kashmir, India. *Journal of Volcanology and Geothermal Research* 138 (3–4), 405–424.
- Harinarayana, T., Abdul Azeez, K., Murthy, D., Veeraswamy, K., Eknath Rao, S., Manoj, C., Naganjaneyulu, K., 2005. Exploration of geothermal structure in Puga geothermal field, Ladakh Himalayas, India by magnetotelluric studies. *Journal of Applied Geophysics* 58 (4), 280–295. doi:10.1016/j.jappgeo.2005.05.005.
- Harrison, T.M., 2006. Did the Himalayan Crystallines extrude partially molten from beneath the Tibetan Plateau? *Geological Society, London, Special Publications* 268 (1), 237–254. doi:10.1144/GSL.SP.2006.268.01.11.
- Herrmann, R.B., Ammon, C.J., 2002. *Computer Programs in Seismology: Surface Waves. Receiver Functions and Crustal Structure*. St. Louis University, St. Louis, MO.
- Hodges, K.V., 2006. A synthesis of the Channel Flow-Extrusion hypothesis as developed for the Himalayan-Tibetan orogenic system. *Geological Society, London, Special Publications* 268 (1), 71–90. doi:10.1144/GSL.SP.2006.268.01.04.
- Hyndman, R.D., Shearer, P.M., 1989. Water in the lower continental crust: modelling magnetotelluric and seismic reflection results. *Geophysical Journal International* 98 (2), 343–365. doi:10.1111/j.1365-246X.1989.tb03357.x.
- Jain, A.K., Manickavasagam, S., Joshi, R.M., Verma, P.K., 2003. HIMPROBE Programme: Integrated Studies on Geology, Petrology, Geochronology and Geophysics of the Trans-Himalaya and Karakoram.
- Jamieson, R.A., Beaumont, C., Medvedev, S., Nguyen, M.H., 2004. Crustal channel flows: 2. Numerical models with implications for metamorphism in the Himalayan-Tibetan orogen. *Journal of Geophysical Research* 109, B06407. doi:10.1029/2003JB002811.
- Jones, T.D., Nur, A., 1984. The nature of seismic reflections from deep crustal fault zones. *Journal of Geophysical Research* 89 (B5), 3153–3171.
- Jones, A.G., Ledo, J., Ferguson, I.J., 2005. Electromagnetic images of the Trans-Hudson orogen: the North American Central Plains anomaly revealed. *Canadian Journal of Earth Sciences* 42, 457–478.
- Kern, H., Popp, T., Gorbatshevich, F., Zharikov, A., Lobanov, K.V., Smirnov, Y.P., 2001. Pressure and temperature dependence of VP and VS in rocks from the superdeep well and from surface analogues at Kola and the nature of velocity anisotropy. *Tectonophysics* 338 (2), 113–134. doi:10.1016/S0040-1951(01)00128-7.
- Klemperer, S.L., 2006. Crustal flow in Tibet: geophysical evidence for the physical state of Tibetan lithosphere, and inferred patterns of active flow. *Geological Society, London, Special Publications* 268 (1), 39–70. doi:10.1144/GSL.SP.2006.268.01.03.
- Kohn, M.J., 2008. P–T–t data from central Nepal support critical taper and repudiate large-scale channel flow of the Greater Himalayan Sequence. *Geol Soc Am Bull* 120 (3–4), 259–273. doi:10.1130/B26252.1.
- Korja, T., Hjelt, S., 1999. The Fennoscandian Shield: a treasure box for deep electromagnetic studies. *Deep Electromagnetic Exploration*. Springer, Berlin/Heidelberg, pp. 31–73. doi:10.1007/BFb0011904.
- Lachenbruch, A.H., Sass, J.H., 1977. Heat flow in the United States and the thermal regime of the crust. In: Heacock, J.G. (Ed.), *The Earth's Crust: Its Nature and Physical Properties*. American Geophysical Union Monograph, vol. 20, pp. 626–675. Washington, DC.
- Leech, M.L., 2008. Does the Karakoram fault interrupt mid-crustal channel flow in the western Himalaya? *Earth and Planetary Science Letters* 276 (3–4), 314–322. doi:10.1016/j.epsl.2008.10.006.
- Li, S., Unsworth, M.J., Booker, J.R., Wei, W., Tan, H., Jones, A.G., 2003. Partial melt or aqueous fluid in the mid-crust of Southern Tibet? Constraints from INDEPTH magnetotelluric data. *Geophysical Journal International* 153 (2), 289–304. doi:10.1046/j.1365-246X.2003.01850.x.
- Litvinovsky, B.A., Steele, I.M., Wickham, S.M., 2000. Silicic magma formation in overthickened crust: melting of Charnockite and Leucogranite at 15, 20 and 25 kbar. *J. Petrology* 41 (5), 717–737. doi:10.1093/ptrology/41.5.717.
- Makovsky, Y., Klemperer, S.L., 1999. Measuring the seismic properties of Tibetan bright spots: evidence for free aqueous fluids in the Tibetan middle crust. *Journal of Geophysical Research* 104 (B5), 10,795–10,826.
- Makovsky, Y., Klemperer, S.L., Ratschbacher, L., Alsdorf, D., 1999. Midcrustal reflector on INDEPTH wide-angle profiles: an ophiolitic slab beneath the India-Asia suture in southern Tibet? *Tectonics* 18 (5), 793–808.
- Nelson, K.D., et al., 1996. Partially molten middle crust beneath Southern Tibet: synthesis of Project INDEPTH results. *Science* 274 (5293), 1684–1688. doi:10.1126/science.274.5293.1684.
- Oliver, J., 1962. A summary of observed seismic surface wave dispersion. *Bulletin of the Seismological Society of America* 52 (1), 81–86.
- Oreshin, S., Kiselev, S., Vinnik, L., Surya Prakasham, K., Rai, S.S., Makeyeva, L., Savvin, Y., 2008. Crust and mantle beneath western Himalaya, Ladakh and western Tibet from integrated seismic data. *Earth and Planetary Science Letters* 271 (1–4), 75–87. doi:10.1016/j.epsl.2008.03.048.
- Rai, S.S., Ashish, A., Padhi, A., Sarma, P.R., 2009. High crustal seismic attenuation in Ladakh-Karakoram. *Bulletin of the Seismological Society of America* 99 (1). doi:10.1785/012007261.
- Rai, S.S., Priestley, K., Gaur, V.K., Mitra, S., Singh, M.P., Searle, M., 2006. Configuration of the Indian Moho beneath the NW Himalaya and Ladakh. *Geophysical Research Letters* 33, L15308. doi:10.1029/2006GL026076.
- Rapine, R., Tilmann, F., Ni, M.W.A.J., Rodgers, A., 2003. Crustal structure of northern and southern Tibet from surface wave dispersion analysis. *Journal of Geophysical Research* 108 (B2), 2120. doi:10.1029/2001JB000445.
- Rosenberg, C.L., Handy, M.R., 2005. Experimental deformation of partially melted granite revisited: Implications for the continental crust. *Journal of Metamorphic Geology* 23 (1), 19–28. doi:10.1111/j.1525-1314.2005.00555.x.
- Shanker, R., Padhi, R.N., Arora, C.L., Prakash, G., Thussu, J.L., Dua, K.J.S., 1976. Geothermal exploration of the Puga and Chumathang geothermal fields, Ladakh, India. *Proceedings, Second United Nations Symposium on the Development and Use of Geothermal Resources, San Francisco, USA, 20–29 May 1975, vol. 1*. US Government Printing Office, Washington DC, pp. 245–258.
- Shapiro, N.M., Ritzwoller, M.H., Molnar, P., Levin, V., 2004. Thinning and flow of Tibetan crust constrained by seismic anisotropy. *Science* 305 (5681), 233–236. doi:10.1126/science.1098276.
- Schulte-Pelkum, V., Monsalve, G., Sheehan, A., Pandey, M.R., Sapkota, S., Bilham, R., Wu, F., 2005. Imaging the Indian subcontinent beneath the Himalaya. *Nature* 435 (7046), 1222–1225. doi:10.1038/nature03678.
- Srivastava, P., Mitra, G., 1994. Thrust geometries and deep structure of the outer and lesser Himalaya, Kumaon and Garhwal (India): implications for evolution of the Himalayan fold-and-thrust belt. *Tectonics* 13 (1), 89–109.
- Takei, Y., 2000. Acoustic properties of partially molten media studied on a simple binary system with a controllable dihedral angle. *Journal of Geophysical Research* 105 (B7), 16,665–16,682.
- Taylor, M.A.J., Singh, S.C., 2002. Composition and microstructure of magma bodies from effective medium theory. *Geophysical Journal International* 149 (1), 15–21. doi:10.1046/j.1365-246X.2002.01577.x.
- Thompson, A.B., Connolly, J.A.D., 1995. Melting of the continental crust: some thermal and petrological constraints on anatexis in continental collision zones and other tectonic settings. *Journal of Geophysical Research* 100 (B8), 15,565–15,579.
- Thussu, J.L., 2002. (compiler) *Geothermal Energy Resources of India*. Geological Survey of India, Special Publication, vol. 69, p. 210.
- Unsworth, M.J., Jones, A.G., Wei, W., Marquis, G., Gokarn, S.G., Spratt, J.E., 2005. Crustal rheology of the Himalaya and Southern Tibet inferred from magnetotelluric data. *Nature* 438 (7064), 78–81. doi:10.1038/nature04154.
- Wang, Y., 2001. Heat flow pattern and lateral variations of lithosphere strength in China mainland: constraints on active deformation. *Physics of the Earth and Planetary Interiors* 126, 121–146. doi:10.1016/S0031-9201(01)00251-5.
- Watanabe, T., 1993. Effects of water and melt on seismic velocities and their application to characterization of seismic reflectors. *Geophysical Research Letters* 20 (24), 2933–2936.
- Weinberg, R.F., Dunlap, W.J., 2000. Growth and deformation of the Ladakh Batholith, Northwest Himalayas: implications for timing of continental collision and origin of calc-alkaline batholiths. *The Journal of Geology* 108 (3), 303–320. doi:10.1086/314405.
- Yin, A., Harrison, T.M., 2000. Geologic evolution of the Himalayan-Tibetan Orogen. *Annual Review of Earth and Planetary Sciences* 28, 211–280. doi:10.1146/annurev.earth.28.1.211.